Inorg. Chem. **2007**, *46*, 4067–4078

Defects in Divided Zinc–Copper Aluminate Spinels: Structural Features and Optical Absorption Properties†

Anne Le Nestour,‡ Manuel Gaudon,‡ Gérard Villeneuve,‡ Marco Daturi,§ Ronn Andriessen,|| and Alain Demourgues*,‡

Institut de Chimie de la Matière Condensée, UPR 9048 CNRS, Université de Bordeaux I, 87 Avenue du Dr. A. Schweitzer, 33608 Pessac Cedex, France, Laboratoire Catalyse et Spectrochimie, UMR 6506, ENSI-Caen, 6 Boulevard Maréchal Juin, 14050 Caen Cedex, France, and Agfa-Gevaert, Septestraat 27, B-2640 Mortsel, Belgium

Received December 15, 2006

$Zn_{1-x}Cu_xAl_2O_4$ ($0 \leq x < 0.30$) compounds have been synthesized by polyesterification using metallic salts and annealing at low temperatures as well as by conventional solid state. XRD-powder data refinements (Rietveld method) have demonstrated that both compound series crystallize in the spinel structure ($Fd\bar{3}m$) and exhibit similar inversion rates. This low-temperature route lead to metastable phases with crystallite sizes around 40 nm whereas particle sizes are larger than 1 μm in the case of solid-state route. This preparative method largely described in the literature allows stabilizing reduced copper states thanks to the presence of reductive organic species, which are decomposed below $T = 700$ °C. The absorption spectra of the $x = 0.15$ composition exhibit strong differences depending on the synthesis route. These differences can be explained by the occurrence of Cu^{2+}/Cu^{+} mixed valencies in compounds prepared by the low-temperature route; 33% of monovalent copper has been identified in the $x = 0.15$ composition prepared by low-temperature process, whereas the solid-state compound contains only divalent copper. Reductive properties of polyesterification reaction implying citric acid and low annealing temperature ($T = 700$ °C) are mainly responsible of the occurrence of the Cu^{2+}/Cu^{+} mixed valencies. Actually, the annealing under air at $T = 1000$ °C of divided zinc–copper aluminates prepared at low temperatures ($T = 700$ °C) leads to the oxidation reaction $Cu^{+} \rightarrow Cu^{2+} + e^{-}$ confirmed by the evolution of magnetic measurements, ESR spectra, and optical absorption properties. Defects such as oxygen vacancies in the anionic network leading to reduction in the cations coordination number could also explain the strong evolution of optical absorption spectra especially around $\lambda = 700$ nm where intervalencies transfer (Cu^{+}/Cu^{2+}) as well as intra-atomic d–d transitions (Cu^{2+} in a 5-fold coordination) can occur. Finally the occurrence of monovalent and divalent copper at the surface of such divided oxides, probably in tetrahedral sites, has been demonstrated by FTIR spectroscopy using the co-adsorption of CO and NO as probe molecules.

Introduction

The stabilization of mixed valencies in Cu-based oxides has been widely studied as well as the impact on electronic properties. Thus, Cu^{2+}/Cu^{+} mixed valencies states have been found in $La_2CuO_{4+\delta}$ or $La_{2-x}Ba_xCuO_4$ adopting perovskite layers networks and exhibiting superconducting behavior (HTC) down to Tc around 40 K.[1,2] Cu^{2+}/Cu^{+} mixed valencies can be also stabilized in $CuY_{1-x}Ca_xAlO_{2+\delta}$, $CuSc_{1-x}Mg_xAlO_{2+\delta}$,[3−6] and $CuBO_{2+\delta}$[7] (B^{3+} are large cations such as La^{3+}) that adopt the delafossite structures deriving from rocksalt network.[8] This is the case of $CuAlO_2$ composi-

* To whom correspondence should be addressed. E-mail: demourg@icmcb-bordeaux.cnrs.fr.

† This paper is dedicated to author Prof. Gérard Villeneuve, who passed away on January 28, 2007.

‡ Université de Bordeaux I.

§ ENSI-Caen.

|| Agfa-Gevaert.

(1) Bednorz, J. G.; Mueller, K. A. *Z. Phys. B* **1986**, *64*, 189.

(2) Radaelli, P. G.; Jorgensen, J. D.; Schultz, A. J.; Hunter, B. A.; Wagner, J. L.; Chou, F. C.; Johnston, D. C. *Phys. Rev. B* **1993**, *48*, 499−510.

(3) Cava, R. J.; Zandbergen, H. W.; Ramirez, A. P.; Takagi, H.; Chen, C. T.; Krajewski, J. J.; Peck, W. F., Jr.; Waszczak, J. V.; Meigs, G.; Roth, R. S.; Schneemeyer, L. F. *J. Solid State Chem.* **1993**, *104*, 437−452.

(4) Duan, N.; Sleight, A. W.; Jayaraj, M. K.; Tate, J. *J. Appl. Phys. Lett.* **2000**, *77*, 1−2.

(5) Trari, M.; Töpfer, J.; Doumerc, J. P.; Pouchard, M.; Ammar, A.; Hagenmuller, P. *J. Solid State Chem.* **1994**, *111*, 104−110.

(6) Van Tendeloo, G.; Garlea, O.; Darie, C.; Bougerol-Chaillout, C.; Bordet, P. *J. Solid State Chem.* **2001**, *2001*, 428−436.

10.1021/ic0624064 CCC: $37.00
Published on Web 04/07/2007

tion adopting the delafossite-type structure[9] and which can be considered as a *p*-type transparent conductive oxide (TCO). In $CuAlO_2$ delafossite, the occurrence of defects with Al^{3+} ions in Cu site and interstitial oxygen atoms forming pseudo-tetrahedral environments around Cu sites (Al_{Cu}"-$2O_i$") has been shown.[10] Thus, most of these mixed valencies Cu-based oxides exhibit unusual electronic properties. In the case of $CuAl_2O_4$ spinel compounds, Cu^{2+} cations occupy both tetrahedral and octahedral sites with an inversion rate close to 35%.[11] This compound exhibits insulating behavior, but the optical absorption spectrum reveals the occurrence of intense bands at the frontier between UV, visible range, and NIR region due to Cu−O charge-transfer band and Cu^{2+} intra-atomic transitions relating to octahedral and tetrahedral fields, respectively.[12] The creation of Cu^{+}/Cu^{2+} mixed valencies into this network should lead to the stabilization of oxygen vacancies. In the spinel structure deriving from the rocksalt type structure, few works dealt with anionic vacancies. This is the case in $LiMn_2O_{4-\delta}$, used as electrodes in secondary batteries, where oxygen nonstoichiometry on solid-state compounds has been measured by thermogravimetric technique depending on the oxygen partial pressure.[13] In $CuMn_2O_4$ spinel, the occurrence of Cu^{+}/Cu^{2+} mixed valencies are compensated by the presence of Mn^{4+} cations leading to the following formula $(Cu^{+}_{0.2}Mn^{2+}_{0.8})[Cu^{2+}_{0.8}Mn^{3+}_{0.2}Mn^{4+}]O_4$ without any oxygen vacancies.[14]

The occurrence of mixed valencies in such aluminates can improve the redox catalytic activity of such oxides, as reported in the literature.[15−17]

In this study, the stabilization of Cu^{+} in Zn−Cu-based aluminates and the creation of defects have been attempted in order to follow the evolution of optical absorption bands in the UV−vis−NIR region associated with electronic transitions involving copper cations. Moreover the stabilization of nanoparticles or metastable phases allows the decrease of Madelung potentials on each site because of the increasing of surface/bulk ratio leading to the reduction of coordination numbers and valence states for cationic sites. A nonconventional synthesis route has been used, phases have been characterized by XRD, and the structures have been refined on the basis of powder XRD data (Rietveld refinement). ESR investigations led to the identification of the Cu^{2+} environments in the $Zn_{1-x}Cu_xAl_2O_4$ series. Finally, magnetic measurements and FTIR studies using probe molecules in order to detect the Cu valence state have been performed.

Experimental Section

Polyesterification reaction based on the Pechini process[18] has been used for the preparation of divided $Zn_{1-x}Cu_xAl_2O_4$, ($0 \le x \le 1$) compounds. This synthesis is based on the polyesterification between a α-hydroxy acids such as citric acid (HO_2C-C(OH)-(CO_2H)-$(CH_2)_2$-CO_2H) and a polyalcohol such as ethylene glycol (HO-CH_2-CH_2-OH) in a metallic solution: Zn^{2+}, Al^{3+}, Cu^{2+}. This mixture was brought to the boil on a hotplate, leading to a solution becoming gradually more and more viscous to finally form a yellowish solid. The latter was then calcinated on a Bunsen burner to get an intermediate black powder. This powder was grounded in an agate mortar and heated up first to $T = 400$ °C for 4 h and then up to $T = 700$ °C for 8 h under air. In this case, the amount of copper, zinc, and aluminum was controlled by atomic absorption (CNRS Vernaison Center). The annealing at low temperature (400 °C, then 700 °C) during short times allows the elimination of all organics, especially carbon species since no traces of carbon have been detected by chemical analysis. This thermal treatment allows us also to keep small size particles with a large content of defects (oxygen/cations vacancies). Moreover in such a process, cations form various complexes and the polyesterification reaction mixes intimately ions with a rather high homogeneity.[18] Based on the Pechini patent and related works,[19] the annealing at $T = 700$ °C during 8 h is enough to get homogeneous compositions and keep nanosized crystallized particles.

The same solid solution has also been synthesized by a solid-state route. Compounds ($Zn_{1-x}Cu_xAl_2O_4$, $0 \le x \le 1$) were prepared starting from binary oxides (CuO, ZnO, and Al_2O_3) of high purity in stoichiometric amounts. The mixtures are heated at 1000 °C during 12 h and slowly cooled down. Several grindings and annealings are necessary to obtain pure phases. Chemical compositions have been controlled by microprobe analysis.

Powder X-ray diffraction patterns have been collected on a Philips X'Pert MPD X-ray diffractometer with Bragg−Brentano geometry, and using Cu $K\alpha_1$ radiation ($5 < 2\theta < 120°$, step of 0.02° and counting time of 30 s) for the compositions prepared by the Pechini route. Solid-state samples were also characterized by X-ray diffraction (XRD) in the same conditions, except the fact that Cu $K\alpha_2$ radiation was used instead of Cu $K\alpha_1$. Diffractogramms have been refined using the Rietveld method with conventional reliability factors.[20] Unit cell parameters, atomic positions, occupancies, and Debye−Waller factors have been refined on the basis of $Fd\bar{3}m$ space group hypothesis corresponding to the spinel structure.

The average particle size and morphology of $Zn_{1-x}Cu_xAl_2O_4$ powders obtained by this low-temperature preparative method were determined by transmission electronic microscopy (TEM, Jeol 2000FX microscope). Size distribution was evaluated from TEM micrographs by manual counting.

Electronic paramagnetic resonance (ESR) spectra have been recorded at $T = 5$ K and at room temperature on a ESR 500 Brucker spectrophotometer working at $\upsilon = 9.449$ GHz in order to identify the local environments of Cu^{2+} ions.

(7) Jacob, A.; Parent, C.; Boutineaud, P.; Le Flem, G.; Doumerc, J. P.; Ammar, A.; Elazhari, M.; Elaatmano, M. *Solid State Commun.* **1997**, *103*, 529−532.
(8) Trari, M.; Topfer, J.; Doumerc, J. P.; Pouchard, M.; Ammar, A.; Hagenmuller, P. *J. Solid State Chem.* **1994**, *111*, 104−110.
(9) Benko, F. A.; Koffyberg, F. P. *J. Phys. Chem. Solids* **1984**, *45*, 57−59.
(10) Ingram, B. J.; Gonzalez, G. B.; Mason, T. O.; Shahriari, D. Y.; Barnabè, A.; Ko, D.; Poeppelmeier, K. R. *Chem. Mater.* **2004**, *16*, 5616−5622.
(11) Otero Arean, C.; Diez Vinuela, J. S.; Rubio Gonzalez, J. M.; Mata Arjona, A. *Mater. Chem.* **1981**, *6*, 165−174.
(12) Pappalardo, R. *J. Mol. Spectrosc.* **1961**, *6*, 554−571.
(13) Sugiyama, J.; Atsumi, T.; Hioki, T.; Noda, S.; Kamegashira, N. *J. Alloys Compd.* **1996**, *235*, 163−169.
(14) Waskowska, A.; Gerward, L.; Staun Olsen, J.; Steenstrup, S.; Talik, E. *J. Phys.: Condens. Matter* **2001**, *13*, 2562.
(15) Valenzuela, M. A.; Aguilar, G.; Bosch, P.; Armenariz, H.; Slals, P.; Montoya, A. *Catal. Lett.* **1992**, *15*, 179.
(16) Marion, M. C.; Garbowski, E.; Primet, M. *J. Chem. Soc. Faraday Trans. I* **1991**, *87*, 1795−1810.
(17) Box, E., Jr. U.S. Patent 3,948,808, 1976.
(18) Pechini, M. P. U.S. Patent 3,330,697, 1967.
(19) Pascual, L.; Gadjov, H.; Kovacheva, D.; Petrov, K.; Herrero, P.; Amarilla, J. M.; Rojas, R. M.; Rojo, M. *J. Electrochem. Soc.* **2005**, *152*, A301.
(20) Rietveld, H. M. *J. Appl. Crystallogr.* **1969**, *2*, 65−71.

Table 1. Rietveld Parameters and Experimental Conditions for Data Collection[a]

	LT	solid-state route
formula	$Zn_{0.85}Cu_{0.15}Al_2O_4$	
symmetry	cubic	
reflection conditions	$h + k = 2n$; $k + l = 2n$; $l + k = 2n$	
space group	$Fd\bar{3}m$ (No. 227)	
unit cell parameters (Å)	8.0825(4)	8.0850(3)
volume (Å^3)	528.00(6)	528.49(3)
Z	8	
radiation	Cu Kα_1	Cu Kα_1, Kα_2
peak shape function	Thompson Cox Hastings	PV = ηL + (1 − η)G
		$\eta = 0.64(2)$
	$H_g = (U + DST^2)\tan^2\theta + V\tan\theta + W + IG/\cos^2\theta$	$H^2 = U\tan^2\theta + V\tan\theta + W$
	$H_l = X\tan\theta + Y/\cos\theta$	$U = 0.006(2)$
	$DST^2 = 0.03(1)$	$V = 0.027(6)$
	$IG = 0$	$W = 0.011(2)$
	$X = 0$, $Y = 0.306(4)$	
measuring range (deg)	$5° < 2\theta < 120°$	
reflections collected	33	33
parameters used in refinement	18	20
CR_p	0.0752	0.128
CR_{wp}	0.0871	0.132
R_{Bragg}	2.40	3.22

[a] Case of $x = 0.15$ composition obtained by the low-temperature preparative method (LT) and solid-state route.

Curie constants of various compositions have been deduced from magnetic susceptibilities ($1/\chi = (T + \theta_p)/C$, $\chi = M/H$) with magnetization recorded between 25 and 200 K (increment 50 K) and magnetic fields H going from 0 to 50 000 Oe. Magnetic measurements have been performed on a S.QU.I.D. detector magnetometer Quantum Design MPMS 5. As the Curie constant is proportional to the concentration of paramagnetic species, Cu^{2+} concentration in the various compounds can be deduced from magnetic data.

The UV−vis−NIR absorption properties were investigated by diffuse reflectance spectroscopy using a Cary 5000E spectrophotometer, with the $210 < \lambda < 2500$ nm wavelength range. Halon standard has been used as a white reference.

Fourier transform infrared (FTIR) studies have been performed on powders outgassed at room temperature with a Nicolet Magna 550 FTIR spectrometer. Probes molecules were introduced at room temperature on the activated samples and then evacuated. The spectra have been treated by the Nicolet MONIC software.

Results and Discussion

Rietveld Analysis of Powder X-ray Diffractograms. The $Zn_{1-x}Cu_xAl_2O_4$ phases ($0 \le x \le 1$) adopt a cubic symmetry with the $Fd\bar{3}m$ space group related to the spinel-type structure. In such a structure, cations can occupy either octahedral sites (16d) or tetrahedral sites (8a) depending on their affinity for these various environments.[21] When all divalent cations are located in tetrahedral sites, the spinel is defined as a normal one or a direct one.[22] In some cases, octahedral sites can also be occupied by a fraction or the totality of divalent cations, forcing an equivalent amount of trivalent cations to occupy tetrahedral sites. In such cases, the spinel structure is partially inverted or fully inverted, respectively. Whatever, octahedral sites in the network are sharing edges and are forming chains, while tetrahedral sites are isolated from each other because they are surrounded by 12 octahedral sites. Each oxygen atom of the network is common to three octahedral sites and one tetrahedral site. Oxygen atoms are located in the 32e site (u, u, u).

X-ray data refinements by the Rietveld method have been performed on the various synthesized $Zn_{1-x}Cu_xAl_2O_4$ compositions in order to determine accurately the oxygen position and site's occupancy. The conditions of data collection have been detailed for the composition $x = 0.15$ in Table 1. While pure phases have been obtained on the whole solid solution for samples prepared by solid-state route,[23] for samples prepared by this low-temperature method with $x \ge 0.30$, traces of parasite phases identified as copper oxide (CuO) or metallic copper (Cu^0) can be stabilized (Figure 1). Moreover, highly divided powders with crystal diameters varying between 10 and 40 nm (Table 2), depending on the copper rate, have been obtained by this low-temperature process; wide X-ray diffraction lines are so observed (Figure 1). Samples issued from solid-state route are not so divided and their X-ray diagrams exhibit narrow diffraction lines. For comparison, Rietveld refinements (experimental, theory, and difference) for the $Zn_{1-x}Cu_xAl_2O_4$ compounds ($x = 0$, 0.15, and 0.30) prepared by both synthesis routes have been represented in Figure 1. Consequently, XRD data refinements for solid-state compounds were led using a pseudo-Voight function deriving from the Caglioti law: $H^2 = U\tan^2\theta + V\tan\theta + W$, whereas the pseudo-Voight Thomson Cox Hastings function was preferred for divided compounds obtained by the Pechini route ($H_g = (U + DST^2)\tan^2\theta + V\tan\theta + W + IG/\cos^2\theta$ and $H_l = X\tan\theta + Y/\cos\theta$) in order to take into account the contribution of particle size on the width of diffraction lines. From the Y term in the Lorentzien contribution can be deduced the crystal size domain of particles. The nanosized feature of the powders obtained by this low-temperature route is illustrated by the transmission electronic micrography performed on the $x = 0.15$ composition obtained by annealing at $T = 700$ °C and

(21) Cornmack, A. N.; Lewis, G. V.; Parker, S. C.; Catlow, C. R. A. *J. Phys. Chem. Solids* **1988**, *49*, 53−57.
(22) Cooley, R. F.; Reed, J. S. *J. Am. Ceram. Soc.* **1972**, *55*, 395−398.
(23) Le Nestour, A.; Gaudon, M.; Villeneuve, G.; Andriessen, R.; Demourgues, A. *Inorg. Chem.* **2007**, *46*, 0000−0000.

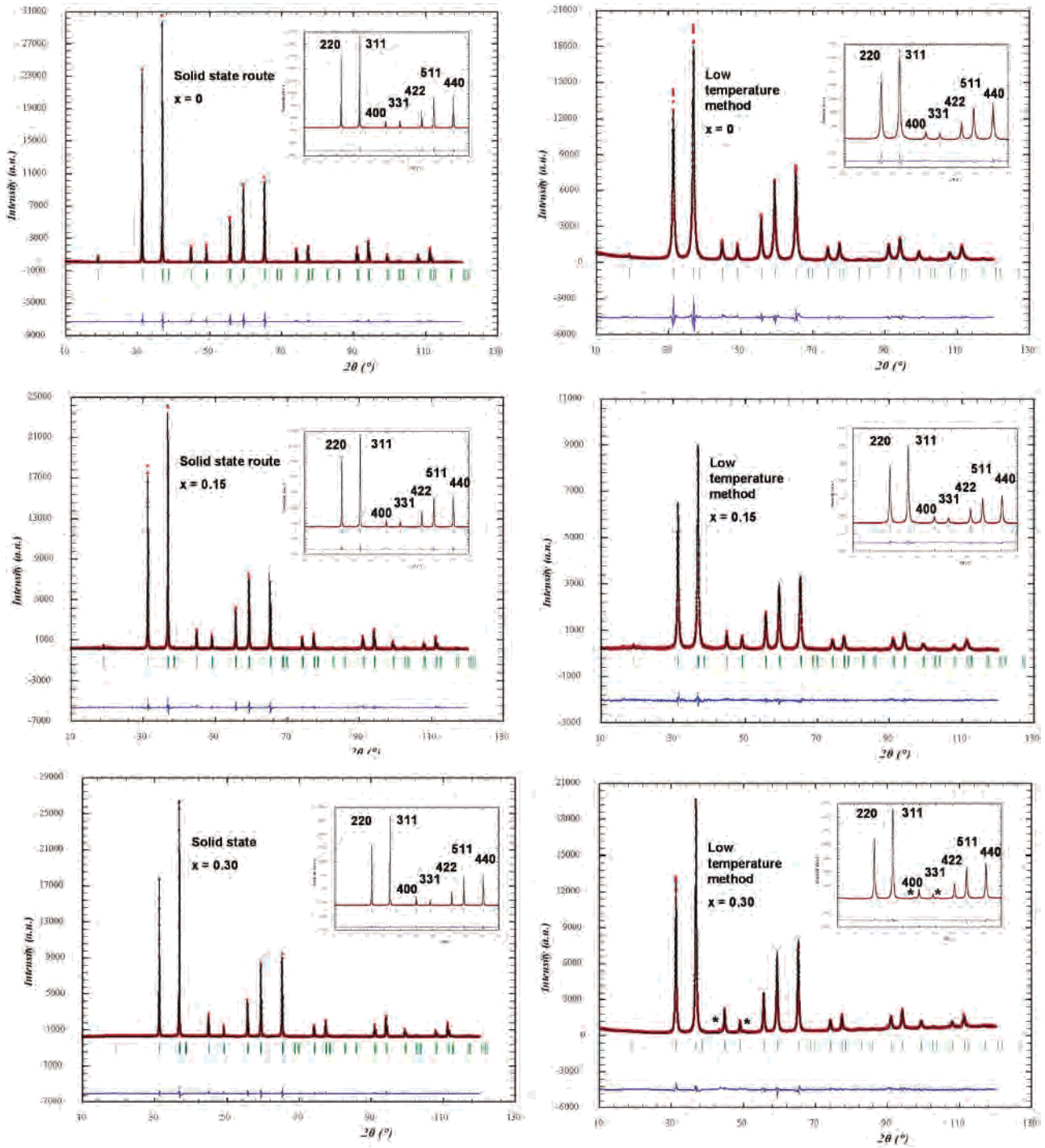

Figure 1. X-ray data refinement by the Rietveld method for the $Zn_{1-x}Cu_xAl_2O_4$ compositions ($x = 0$, $x = 0.15$, and $x = 0.30$) obtained by solid-state route and low-temperature preparative method.

Table 2. Crystal Size Domains Estimated by XRD Analysis and TEM Observation (JEOL, 200 keV) for Various Compositions $Zn_{1-x}Cu_xAl_2O_4$ Prepared by the Low-Temperature Preparative Method

x in $Zn_{1-x}Cu_xAl_2O_4$	0.15	0.20
τ (nm) estimated by XRD	19.4(4)	21(1)
τ (nm) measured by TEM	40	35

after thermal treatment at $T = 1000$ °C (Figure 2), showing that annealing at high temperature does not affect the size and morphology.

The atomic positions, isotropic thermal displacements, occupancies of each site, and reliability factors (R_p, R_{wp}, R_{Bragg}) for $x = 0$, $x = 0.15$, and $x = 0.30$ synthesized by esterification process and solid-state route are reported in Table 3. Compositions with $x \geq 0.30$ did not result in pure phases by this low-temperature process, and only the case of $x = 0.30$ is reported.

One should have to point out that, whatever the x copper content, the lattice parameter corresponding to the low-temperature process is systematically smaller than for the composition obtained by solid-state route. Moreover, whereas the a parameter for compositions obtained by solid-state route is almost identical for $0 < x < 0.30$, the cell parameter

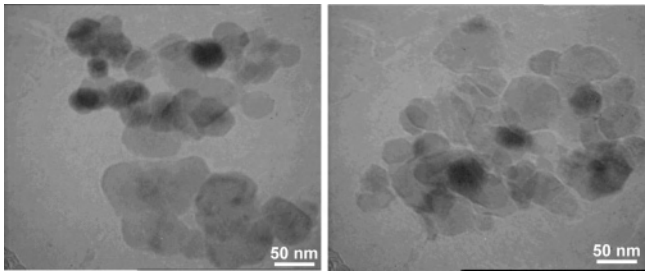

Figure 2. Transmission electronic micrographs of the composition $x = 0.15$ prepared by low-temperature preparative method just after synthesis (left) and after annealing at $T = 1000$ °C under air for 12 h (right).

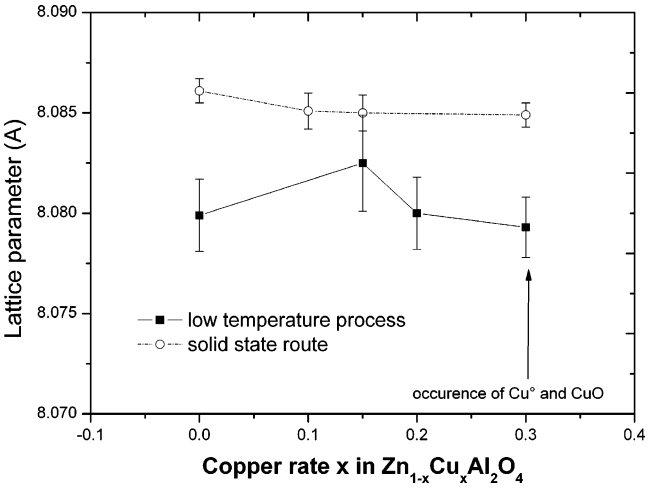

Figure 3. Variation of the lattice parameter for the various $Zn_{1-x}Cu_xAl_2O_4$ compositions obtained by both synthesis routes (NB: for the low-temperature preparative method, only pure phases are obtained for $x < 0.30$).

corresponding to compositions obtained by this low-temperature method exhibits stronger variations despite the standard deviation values, passing through a maximum at $x = 0.15$ and strongly decreasing up to 8.079 Å for $x = 0.30$ while for $CuAl_2O_4$ obtained by solid-state route, the cell parameter is equal to 8.078 Å[23] (Figure 3).

This gradual decreasing of the cell parameter is directly linked, in a first approach, to the introduction of Cu^{2+} cations in the network instead of Zn^{2+} cations, copper cations being smaller than zinc cations[24] and more polarizing as well in a 4-fold or 6-fold coordination.

Structural refinements on both the series indicate also a similar variation of the oxygen position in the 32 e site versus the copper rate x in the spinel.[23] This result indicates that the cation−oxygen distances in 8a and 16d sites of the spinel network evolve in the same manner whatever the preparation mode.

$ZnAl_2O_4$ is always described in the literature as a normal spinel (Zn^{2+} cations are located in 8a sites, and Al^{3+} cations are occupying 16d sites).[22] For some examples, a small inversion is observed in cases of samples prepared by alternative synthesis routes[25] such as sol−gel or hydrothermal routes. Calculations based on normalized ion energy method also show that inversion in $ZnAl_2O_4$ is not energetically favorable.[26] In the case of compounds prepared by the Pechini process,[18] an inversion of 8% (1) has been found by XRD data refinement, whereas an inversion rate of 3% (1) has been refined in the case of solid-state route.[23] The observed inversion rate in $ZnAl_2O_4$ (∼8%) prepared by this low-temperature method can be understood as a consequence of the nanosized effect on the cationic distribution leading to a stabilization of a larger amount of Al^{3+} cations in tetrahedral sites. Nevertheless, a ^{27}Al MAS NMR study on the $ZnAl_2O_4$ compounds prepared by this preparative method has revealed a comparatively weaker amount of 4-fold coordinated Al^{3+} cations (around 2%). This study indicates on the other hand the occurrence of 5-fold coordinated Al^{3+} cations (around 4%) in the compound, suggesting the presence of oxygen vacancies and, consequently, the presence of locally rearranged coordination sites around the defects. Actually this low-temperature method leads to the formation of nanoparticles where Al^{3+} cations can be found with a lower coordination number than in octahedral sites as reported in direct spinel $ZnAl_2O_4$ prepared by solid-state route. The preparation of nanoparticles allows forcing polarizing cations such as Al^{3+} ions to reduce their Madelung potential and then to adopt tetrahedral or 5-fold coordinated sites into the spinel framework. This is the reduction of Madelung energy into zinc aluminate nanoparticles that leads to the creation of defects such as oxygen vacancies.

Cu^{2+} cations are known to be preferentially stabilized in octahedral coordination than in tetrahedral one.[27] That is essentially why partially inverted structures were expected for $Zn_{1-x}Cu_xAl_2O_4$ ($x \neq 0$). However, Cu^{2+} cations have a $3d^9$ electronic configuration, leading the octahedral coordination to a strongly stabilized distorted octahedron due to the Jahn−Teller effect of this $3d^9$ configuration. For the spinel structure, it has been already demonstrated that a limited Jahn−Teller cooperative distortion was supported by the network.[14] Pure $CuAl_2O_4$ obtained by solid-state route is not indeed a totally inverted spinel, but its inversion is limited to around 35%.[28] Electronic and sterical effects leading to the stabilization of Cu^{2+} cations in tetrahedral and octahedral sites are mainly responsible for this limited inversion rate. The evolution of structural features as well as optical absorption properties of the $Zn_{1-x}Cu_xAl_2O_4$ solid solution obtained by solid-state route at high-temperature ($T = 1000$ °C) have been described and discussed in a recent paper.[23]

In the solid solution, $Zn_{1-x}Cu_xAl_2O_4$, Zn^{2+} ions are assumed to occupy mainly tetrahedral sites while other cations have a strong preference for octahedral coordination. The inversion rates corresponding to the Al occupancy in tetrahedral sites are given in Table 3. In the case of spinels synthesized by esterification reaction considering that zinc cations occupy tetrahedral sites, the copper content in

(24) Shannon, R. D. *Acta Crystallogr. A* **1976**, 751.
(25) Van der Laag, N. J.; Snel, M. D.; Magusin, P. C. M. M.; De With, G. *J. Eur. Ceram. Soc.* **2004**, *24*, 2417−2424.
(26) Grimes, R. W.; Anderson, A. B.; Heuer, A. H. *J. Am. Chem. Soc.* **1989**, *111*, 1−7.
(27) Burns, R. G. *Mineralogical Applications of Crystal Field Theory*; Syndics of the Cambridge University Press: Cambridge, 1970.
(28) Otero Arean, C.; Diez Vinuela, J. S. *J. Solid State Chem.* **1985**, *60*, 1−5.

Table 3. Atomic Positions, Isotropic Thermal Displacements, and Reliability Factors of the Various $Zn_{1-x}Cu_xAl_2O_4$ Compositions (Powder Rietveld Analysis)

$ZnAl_2O_4$ ($Fd\bar{3}m$), X-ray Refinement

atoms	site	x	y	z	biso	occupancies
Low-Temperature Preparative Method (a = 8.0799(6) Å, CR_p = 8.97%, CR_{wp} = 9.81%, R_{Bragg} = 3.65)						
Zn1	8a	1/8	1/8	1/8	0.665(66)	0.920(10)
Al1	8a	1/8	1/8	1/8	0.665(66)	0.080(10)
Zn2	16d	1/2	1/2	1/2	0.66(12)	0.039(6)
Al2	16d	1/2	1/2	1/2	0.66(12)	0.960(6)
O	32e	0.2639(5)	0.2639(5)	0.2639(5)	0.46(16)	1
Solid-State Route (a = 8.0861(2) Å, CR_p = 10.6%, CR_{wp} = 14.3%, R_{Bragg} = 4.44)						
Zn1	8a	1/8	1/8	1/8	0.79(7)	0.967(3)
Al1	8a	1/8	1/8	1/8	0.79(7)	0.033(3)
Zn2	16d	1/2	1/2	1/2	0.79(10)	0.016(2)
Al2	16d	1/2	1/2	1/2	0.79(10)	0.984(2)
O	32e	0.2649(3)	0.2649(3)	0.2649(3)	0.74(14)	1

$Zn_{0.85}Cu_{0.15}Al_2O_4$ ($Fd\bar{3}m$), X-ray Refinement

atoms	site	x	y	z	biso	occupancies
Low-Temperature Preparative Method (a = 8.0825(4) Å, CR_p = 7.52%, CR_{wp} = 8.71%, R_{Bragg} = 2.40)						
Zn1/Cu1	8a	1/8	1/8	1/8	0.91(8)	0.92(1)
Al1	8a	1/8	1/8	1/8	0.91(8)	0.08(1)
Cu2	16d	1/2	1/2	1/2	1.00(15)	0.040(6)
Al2	16d	1/2	1/2	1/2	1.00(15)	0.960(6)
O	32e	0.2636(4)	0.2636(4)	0.2636(4)	0.61(17)	1
Solid-State Route (a = 8.0850(3) Å, CR_p = 12.8%, CR_{wp} = 13.2%, R_{Bragg} = 3.22)						
Zn1/Cu1	8a	1/8	1/8	1/8	1.104(68)	0.918(9)
Al1	8a	1/8	1/8	1/8	1.104(68)	0.082(9)
Cu2	16d	1/2	1/2	1/2	1.06(11)	0.040(5)
Al2	16d	1/2	1/2	1/2	1.06(11)	0.960(5)
O	32e	0.2636(4)	0.2636(4)	0.2636(4)	1.11(15)	1

$Zn_{0.70}Cu_{0,30}Al_2O_4$ ($Fd\bar{3}m$), X-ray Refinement (Presence of CuO and Cu^0 as Impurities)

atoms	site	x	y	z	biso	occupancies
Low-Temperature Preparative Method (a = 8.0793(5) Å, CR_p = 10.6%, CR_{wp} = 10.9%, R_{Bragg} = 2.96)						
Zn1/Cu1	8a	1/8	1/8	1/8	1.20(12)	0.84(2)
Al1	8a	1/8	1/8	1/8	1.20(12)	0.16(2)
Cu2	16d	1/2	1/2	1/2	1.36(20)	0.082(9)
Al2	16d	1/2	1/2	1/2	1.36(20)	0.918(9)
O	32e	0.2631(7)	0.2631(7)	0.2631(7)	0.74(23)	1
Solid-State Route (a = 8.0849(2) Å, CR_p = 13.6%, CR_{wp} = 12.0%, R_{Bragg} = 2.43)						
Zn1/Cu1	8a	1/8	1/8	1/8	0.761(49)	0.846(8)
Al1	8a	1/8	1/8	1/8	0.761(49)	0.154(8)
Cu2	16d	1/2	1/2	1/2	0.681(73)	0.077(4)
Al2	16d	1/2	1/2	1/2	0.681(73)	0.923(4)
O	32e	0.2634(3)	0.2634(3)	0.2634(3)	0.81(10)	1

tetrahedral and octahedral sites remains identical, whatever the copper rate x for $0 < x < 0.30$. In the case of the solid-state route, the copper content in tetrahedral and octahedral sites seems also identical, but the copper rate in tetrahedral sites slightly increases for $x > 0.40$ and becomes equal to 65% for $CuAl_2O_4$. Above the composition $x = 0.60 \approx 4/7$, the preferential coordination for copper switches from the octahedral environment to the tetrahedral one. In these conditions, the maximal steric constrains associated to the Jahn−Teller distortion are reached, so that Cu^{2+} cations cannot occupy additional octahedral sites.[23] Moreover, in the case of the low-temperature method, the formation of copper metal and CuO oxide is observed for x Cu content higher than $x = 0.30$.

The reductive conditions of the polyesterification process implying citric acid and ethylene glycol could explain first the formation of Cu^+ cations in tetrahedral environment, followed by the disproportionation reaction

$$2Cu^+ \rightarrow Cu^0 + Cu^{2+} \quad (1)$$

as the copper rate is larger than or equal to $x = 0.30$, because of the occurrence of strong steric and electronic constrains. This hypothesis will be discussed in the following paragraphs. The larger decreasing of the cell parameter for $0.15 < x < 0.30$ compositions prepared by this low-temperature process can be attributed to the formation of a larger defect rate such as anionic vacancies associated or not to cationic vacancies and to the evolution of Cu valence state as the copper content increases. The formation of smaller size particle leads to generation of also smaller oxidation states at the surface due to the reduction of Madelung energy and higher defects concentration. Thus for $0 < x < 0.15$, the increase of the cell parameter is probably associated to the formation of Cu^+, Cu^{2+} mixed valencies with anionic vacancies and for $0.15 < x < 0.30$, the gradual decreasing of cell parameter is probably due to the evolution of Cu valence state.

UV−Vis−NIR Absorption Properties. As the particle sizes are largely lower than the UV−vis−NIR wavelengths, the transformation of diffuse reflectance by the Kubelka−Munk equation was not applicable in the case of spinels obtained by this low-temperature method. Then, the reflec-

tance spectra are converted into absorbance by considering the optical density given by the relationship: $DO = -\log(R)$.

Correlation between structural features and absorption properties for $Zn_{1-x}Cu_xAl_2O_4$ obtained by solid-state route has been developed in detail in a recent paper.[23] Because of two coordination numbers for copper cations in spinel network, two intra-atomic d−d transitions related to copper(II) in octahedral and tetrahedral sites are expected ($t_2 \rightarrow e$ and $e \rightarrow t_2$, respectively). Octahedral transition occurs with a weak probability, because distorted octahedral sites in spinels (D_{3d}) are "pseudo-centrosymmetric" whereas tetrahedral transition takes place with an exalted intensity since the coordination state does not exhibit a centrosymmetry character. These two intra-atomic d−d transitions are located at around 750 and 1500 nm, respectively, in good agreement with the expected crystal field values in octahedral and tetrahedral sites ($\Delta_{Td} \approx 4/9\Delta_{Oh}$). Two other absorption bands assigned to interatomic charge transfers between oxygen and cationic species in octahedral and tetrahedral sites are also presented. These two bands are located in the UV and at the frontier between UV and visible range, 250 and 450 nm, respectively. One should have to note that for $0 \leq x \leq 0.20$, only the $x = 0.15$ composition exhibits the stronger difference between the two routes. This point will be discussed in the following part for instance. The phases corresponding to $0.20 \leq x < 0.30$ show smaller variations of the absorption spectra whatever the synthesis route (Figure 4a,b) as compared to the $x = 0.15$ composition.

Both the expected absorption bands (interatomic charge transfers and intra-atomic d−d transitions) are presented for the compounds obtained by low-temperature process. Their positions are also compatible with electronic transitions observed for the solid-state compounds.[23] Nevertheless some anomalies can be detected concerning their observed intensities. It is especially remarkable for the absorption band assigned to the intra-atomic d−d transition relative to Cu^{II} in octahedral sites, whose the strong intensity is not compatible with the Laporte selection rules. This effect is much more affected for the low copper rates x in $Zn_{1-x}Cu_xAl_2O_4$. It is particularly clear for the $x = 0.15$ composition when absorption spectra of the composition obtained by the low-temperature [(LT) sample in the rest of the text] and by the solid-state route [(S) sample in the rest of the text] are compared (see Figure 4, panels a and b).

As far as the $x = 0.15$ composition is concerned, the optical properties are clearly function of the synthesis route. Especially, the absorption band spreading from 600 to 1100 nm for the (LT) sample occurs in the same wavelength range as the intra-atomic d−d transition relative to Cu^{II} in octahedral site. Various hypotheses can be proposed in order to explain the strong variation of the absorption band intensity centered at around 750 nm: (1) a strong evolution of the inversion rate with the synthesis route; (2) a higher distortion of octahedral sites in (LT) sample than in the (S) sample; (3) the occurrence in the (LT) sample of new species giving intra-atomic transitions in this energy range, which can be due to the stabilization of nanoparticles as well as

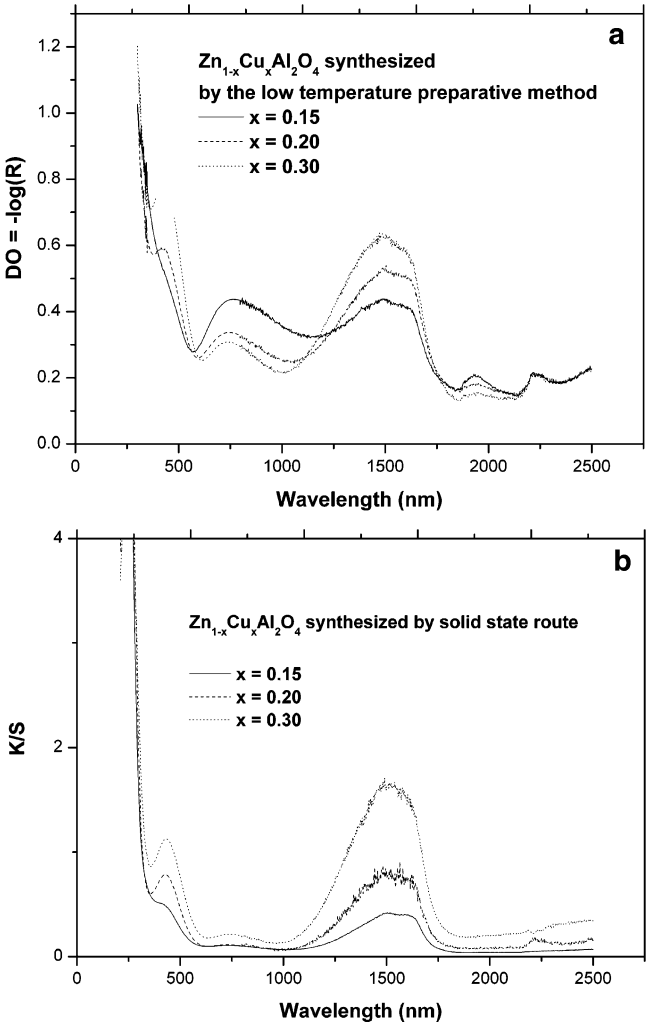

Figure 4. Comparison of the optical absorption properties for the composition with $x = 0.15$ (—), $x = 0.20$ (- - -), and $x = 0.30$ (···) synthesized by the low-temperature preparative method (a) and by the solid-state route (b).

the reductive conditions leading to the creation of anionic and/or cationic vacancies. (3a) Monovalent copper cations Cu^+ can lead to intra-atomic $3d^{10} \rightarrow 4s^0$ transitions in Cu-based oxides as in $CuAlO_2$ delafossite where the transition occurs below 780 nm.[29] (3b) Around the oxygen vacancies, the formation of Cu^{2+} in a 5-fold coordination, such as in RE_2BaCuO_5 (RE = Y, Sm, Gd) with a C_{4v} symmetry, leading to strong absorption around 700 nm.[30] (3c) Interatomic Cu^{II}/Cu^{I} intervalencies transfers occurring between 775 and 1000 nm could also explain such behavior.[31]

The first hypothesis can be easily excluded thanks to the X-ray data refinements, which show that whatever the synthesis route, X-ray diagrams corresponding to the same copper content are refined with almost the same inversion rate. For instance for $x = 0.15$, the refined inversion rate is $\gamma \approx 8\%$ as well in (LT) and (S) samples.

(29) Ammar, A.; Wichainchai, A.; Doumerc, J. P.; Pouchard, M.; Hagenmuller, P. *C. R. Acad. Sci. Ser. II: Mech., Phys., Chim., Sci. Univers, Sci. Terre* **1986**, *303*, 353−356.
(30) Michel, C.; Raveau, B. *J. Solid State Chem.* **1982**, *43*, 73−80.
(31) Patel, R. N.; Kumar, S.; Pandeya, K. B. *Indian J. Chem.* **2001**, *40A*, 1104−1109.

Table 4. ESR Measurements (g values, hyperfine constants, and signal width) Compared to Absorption Properties of Cu^{2+} in Distorted Octahedral Site with D_{2h} Point Group (Case of $x = 0.15$)

octahedra axis	x	y	z
experimental g values	2.072	2.135	2.335
hyperfine constants (Gauss)	20	70	130
signal width (LT)	20	40	30
signal width (S)	80	120	100
expected optical transitions[a] (nm)	420	800	500
observed optical transitions (nm)	between 600 and 800 nm		

[a] $\Delta_x = 2\lambda/(g_x - g_e)$; $\Delta_y = 2\lambda/(g_y - g_e)$; $\Delta_z = 8\lambda/(g_z - g_e)$ with $\lambda_{Cu} = 830\ cm^{-1}$ (spin−orbit coupling for isolated copper[37]) and $g_e = 2$ (Landé factor for isolated electron).

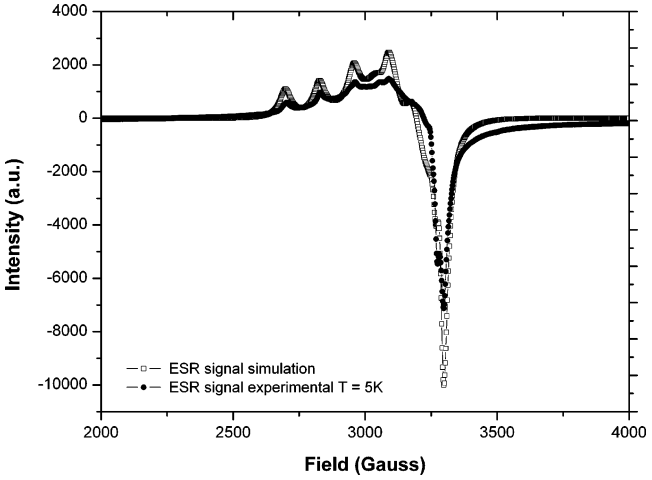

Figure 5. ESR signal and ESR simulation for $Zn_{1-x}Cu_xAl_2O_4$ ($x = 0.15$) compounds synthesized by the low-temperature preparative method.

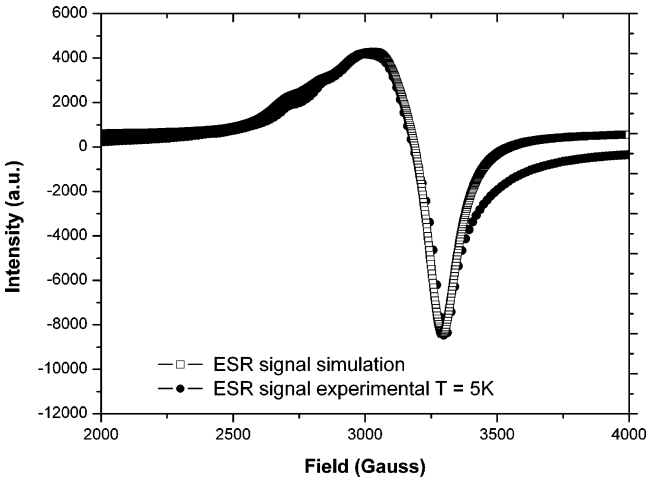

Figure 6. ESR signal and ESR simulation for $Zn_{1-x}Cu_xAl_2O_4$ ($x = 0.15$) compounds synthesized by solid-state route.

ESR Investigations. Concerning the second hypothesis, an ESR study at room temperature as well as $T = 5$ K on the $Zn_{1-x}Cu_xAl_2O_4$ compositions with $x = 0.15$ obtained from both the synthesis routes lead after simulation (Table 4) to the same orthorhombic distortion ($g_x = 2.072$, $g_y = 2.135$, $g_z = 2.335$) for Cu^{2+} in octahedral sites (Figures 5 and 6). Only ESR spectra recorded at $T = 5$ K have been reported because of their best resolution. Actually, the octahedral environment for Cu^{II} cations exhibits the same distortion whatever the synthesis route and these sites can be considered as centrosymmetric (D_{2h} symmetry).

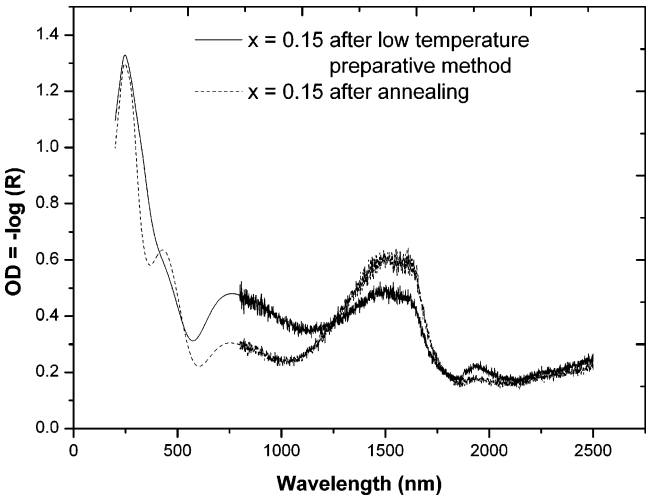

Figure 7. Effect of an annealing at $T = 1000$ °C on the absorption properties of the $Zn_{1-x}Cu_xAl_2O_4$ compound with $x = 0.15$ prepared by the low-temperature preparative method.

Based on these conclusions, the occurrence of a mixed valency for copper cations in the (LT) compounds can be strongly considered. And this is even more probable that the reductive conditions of process implying citric acid are obvious. The stabilization for high copper content ($x \geq 0.30$) of CuO and metallic copper, resulting probably from the disproportionation reaction of monovalent copper is indeed in good agreement with the occurrence of Cu^+ cations in compounds prepared by this low-temperature method.

An annealing under air at $T = 1000$ °C of the various compositions $Zn_{1-x}Cu_xAl_2O_4$ synthesized by this low-temperature process has resulted in the strong attenuation of the absorption band located between 600 and 1100 nm without any changes of morphology and size particles (Figure 2). The effect of annealing under air on the absorption properties of the composition with $x = 0.15$ (leading to sample (A)) is illustrated at the Figure 7. Moreover, the increase of the absorption band around 1500 nm due to Cu^{II} in tetrahedral site after annealing can also be noticed. The annealing under air at 1000 °C lead surprisingly to the elimination of oxygen vacancies associating to the oxidation reaction $2Cu^+ + {}^1/_2O_2 \rightarrow 2Cu^{2+} + O^{2-}$. Then the annealing implies an oxidation of monovalent copper cations present initially in the structure, where these latters were probably stabilized in tetrahedral sites, which is in good agreement with the preferential environments of Cu^+ cations[32] and the increase after annealing of the absorption band located at around 1500 nm related to Cu^{2+} cations in tetrahedral sites.

In the same time, the annealed compound at $T = 1000$ °C (sample (A)) has been characterized by electronic paramagnetic resonance and the obtained ESR signal has been compared to the pristine material. Both ESR signals are superposed in Figure 8, and the simulation of the ESR signal for Cu^{II} in octahedral site for sample (A) is represented on the Figure 9. The g values proposed by the ESR simulation of both samples (before and after annealing) are equivalent and estimated to $g_x = 2.072$, $g_y = 2.135$, and $g_z = 2.335$

(32) Smit, J. *Solid State Commun.* **1968**, *6*, 745−746.

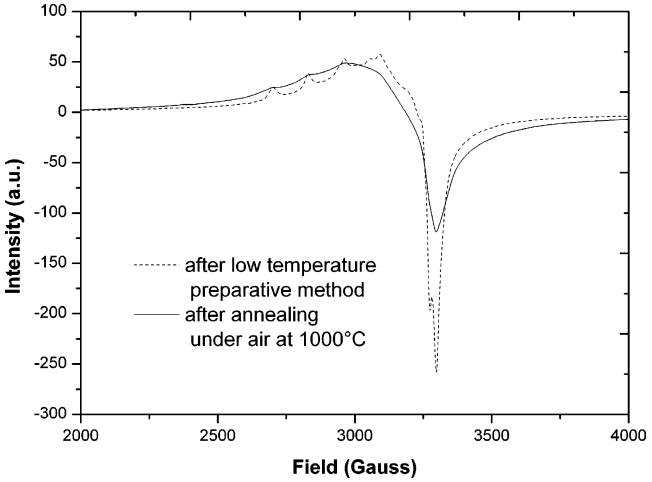

Figure 8. Variation of the ESR signal for the composition $Zn_{1-x}Cu_xAl_2O_4$ ($x = 0.15$) just after the low-temperature preparative method (− −) and after the annealing (−).

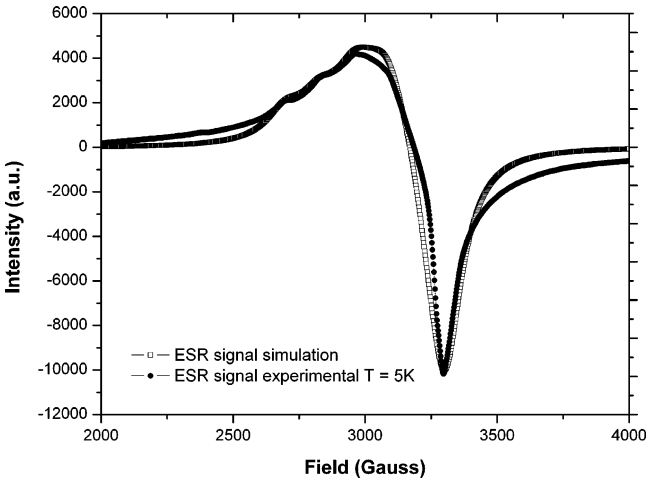

Figure 9. ESR spectrum simulation for $x = 0.15$ (low-temperature preparative method) after annealing.

(Table 4). Concerning the signal width in the three dimensions, the estimated values after annealing are much higher than those estimated before the thermal treatment ($W_x = 20$ G, $W_y = 40$ G, and $W_z = 30$ G for LT sample and $W_x = 80$ G, $W_y = 120$ G, and $W_z = 100$ G for A sample). An increasing of the concentration in paramagnetic species (Cu^{2+} cations) results usually in the broadening of the ESR signal and to the progressive disappearance of the hyperfine structure.[33] Consequently, the hypothesis of an oxidation of Cu^{+} into Cu^{2+} during annealing is in good agreement with the evolution of the ESR signals detected for both the samples before and after annealing. Moreover, one should have to point out that the ESR signal corresponding to $x = 0.15$ prepared by esterification process is quite similar with that of $x = 0.10$ composition obtained by solid-state route (Figure 10), containing smaller amount of Cu^{2+} cations.

Magnetic Measurements. Finally, magnetic measurements have been performed in order to evaluate the concentration of divalent copper cations in the esterification compounds before and after annealing. The Cu^{2+} contents

(33) Thorp, J. S.; Skinner, A. R. *J. Magn. Magn. Mater.* **1987**, *69*, 34−42.

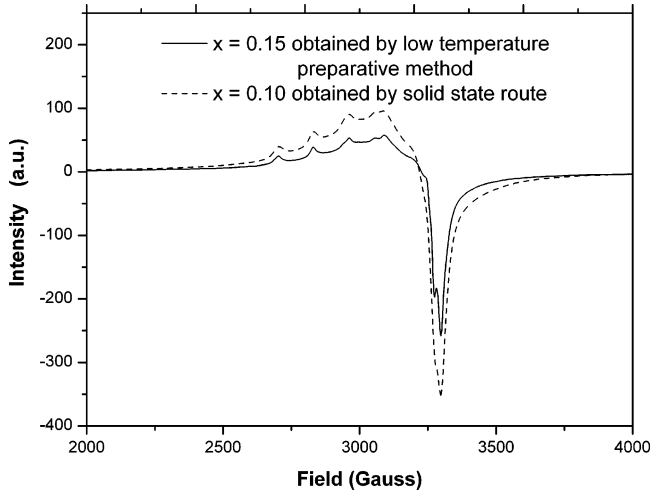

Figure 10. Comparison between ESR signals of $x = 0.15$ composition obtained by low-temperature preparative method and $x = 0.10$ composition obtained by solid-state route.

Table 5. Magnetic Measurements on Various $Zn_{1-x}Cu_xAl_2O_4$ Compositions Obtained by the Low-Temperature Preparative Method and Solid-State Route

x in $Zn_{1-x}Cu_xAl_2O_4$	0.150	0.200	0.300 (ϵ Cu, CuO)
Low-Temperature Preparative Method (LTPM)			
C (mol^{-1})	0.0484(4)	0.0850(6)	0.1249(9)
x' (Cu^{2+}) on the basis of C_{Cu} = 0.4470 mol^{-1}	0.108(1)	0.190(3)	0.279(4)
$\lvert\theta p\rvert$ (K)	5.2(2)	11.9(2)	19.0(3)
Low-Temperature Preparative Method Followed by Annealing under Air at 1000 °C (12 h)			
C (mol^{-1})	0.0649(4)	0.0876(6)	0.1277(9)
x' (Cu^{2+}) on the basis of C_{Cu} = 0.4470 mol^{-1}	0.145(2)	0.196(3)	0.286(4)
$\lvert\theta p\rvert$ (K)	16.2(2)	15.6(2)	20.3(3)
Solid-State Route			
C (mol^{-1})	0.0661(5)	NA[a]	NA
x' (Cu^{2+}) on the basis of C_{Cu} = 0.4470 mol^{-1}	0.148(2)	NA	NA
$\lvert\theta p\rvert$ (K)	19.3(3)	N.A	NA

[a] NA, not available.

are summarized in Table 5. These measurements clearly show that the annealing under air implies the oxidation of copper species whose oxidation state was lower than +II. Furthermore, the systematic increase of θ_p parameter and exchange integral J ($J = \theta_p/k$) after annealing for any composition indicates also the reinforcement of Cu^{2+}/Cu^{2+} antiferromagnetic interactions. Moreover it is relevant to point out that for $x = 0.30$ and $x = 0.20$ for instance, whatever the synthesis route, the Curie constants remains similar with majority of Cu^{2+} cations (Table 5) despite the occurrence of small amount of Cu^{0} for $x = 0.30$ sample. It has to be noticed that the mixed valency is much more stabilized for the composition with $x = 0.15$. Then on the basis of the determination of the Cu^{2+} content in $x = 0.15$ compounds and considering the inversion rate on the basis of the powder XRD Rietveld refinement, 33% of copper are in +I state and occupy a tetrahedral site. Moreover, as pointed out by the ESR measurements, the magnetic behavior of sample (A) is very different from the one of samples prepared by low-temperature process, but it is quiet identical

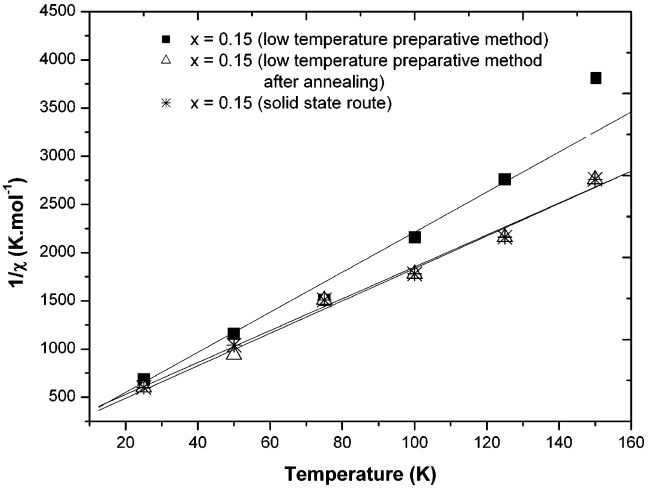

Figure 11. Inverse of magnetic susceptibility vs temperature for the composition with $x = 0.15$ obtained by low-temperature preparative method, before and after annealing and by solid-state route. (Linear fits are also represented.)

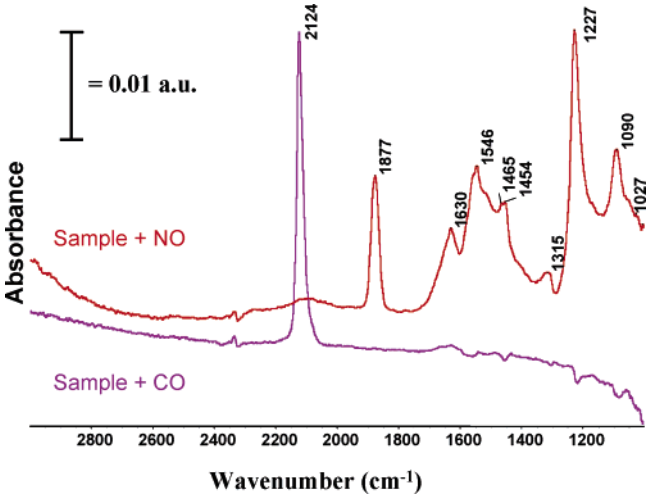

Figure 12. FTIR spectra with co-adsorption (CO and NO) for the composition with $x = 0.15$.

to the one of solid-state sample, since their Curie−Weiss fits are identical (Figure 11). Moreover, the evolution of the cell parameter determined for $x = 0.15$ and $x = 0.20$ compositions for instance before and after annealing under air at $T = 1000$ °C has been also analyzed. If the cell parameter decreases from $a = 8.0825(4)$ Å to $a = 8.0810(3)$ Å for $x = 0.15$ composition due to the oxidation reaction $Cu^+ \rightarrow Cu^{2+} + e^-$, it remains constant $a = 8.0800(8)$ Å for $x = 0.20$ composition whatever the annealing temperature, in good agreement with the fact that for this composition a majority of divalent copper has been identified.

Absorption properties, ESR signals, and magnetic measurements have clearly demonstrated the presence of monovalent copper stabilized within the spinel network issued from esterification route. Moreover the post-annealing step performed on these samples clearly underlined that the presence of Cu^+ cations results from the occurrence of oxygen vacancies as defects stabilized into these nanoparticles. Then, surprisingly, the treatment under air at $T = 1000$ °C allows eliminating these defects leading to the oxidation reaction $Cu^+ \rightarrow Cu^{2+} + e^-$.

Assuming that zinc atoms occupy preferentially tetrahedral sites and that copper ions are half-distributed between tetrahedral and octahedral sites (since inversion rate is almost equal to 50% for $0 < x < 0.30$), at $x = 1/6$, the amount of copper cations occupying tetrahedral sites is equal to 1/12, and the same amount is located in octahedral sites. Then, considering that each tetrahedral site is surrounded by twelve octahedral sites, the probability to get isolated Cu−Cu pairs becomes high. This situation leads probably to stabilize a large amount of Cu^+ cations into these pairs considering electrostatic interactions d^9-d^{10}.

Moreover, at around $x = 1/6$, the "a" parameter cell pass through a maximum ($a = 8.0825$ (4) Å) corresponding to the largest amount of Cu^+ idientified by magnetic measurements. For higher copper contents, the extension of copper−copper interactions results in the destabilization of Cu^+ sites and the stabilization of divalent copper on the basis of steric and electrostatic considerations. Furthermore, Cu^+ as well as Cu^{2+} cations can be easily stabilized in tetrahedral environments, then the reduction of oxygen vacancies and the oxidation of Cu^+ as well as the rearrangement around oxygen vacancies become more favorable. Because of the evolution of the cell parameter in this series, the occurrence of oxygen as well as cationic vacancies has been proposed. This is due to the reduction of Madelung potentials for both oxygen and cationic sites in these nanoparticles taking into account the large surface/bulk ratio. The as-prepared metastable phases evolve at high temperatures to the thermodynamically stabilized compound although the particles size does not change with this final thermal treatment at $T = 1000$ °C.

FTIR Surface Spectroscopy by Adsorption of Probe Molecules for Surface Cu^+ Species Identification. In order to demonstrate directly the occurrence of Cu^+ species in $Zn_{1-x}Cu_xAl_2O_{4-\delta}$ spinels, FTIR studies have been performed. Cu^{2+} and Cu^+ cations located at the surface of a material can be easily identified by FTIR spectroscopy with probe molecules. Especially co-adsorption of nitrogen monoxide and carbon monoxide leads to identify the oxidation state of copper at the surface of materials.

Nitrogen monoxide (NO) can be indeed adsorbed on surface containing various copper species under several forms,[34] but nitrosyl groups (-NO) are unstable with Cu^+ cations. In the same time, carbon monoxide can be also adsorbed on surface with various copper species, but carbonyl groups are unstable with Cu^{2+} cations.[35]

Various adsorbed molecules on Cu sites have been characterized by vibration wavenumbers. This study has been performed on the composition with $x = 0.15$ initially outgassed under vacuum. The FTIR spectra after NO and CO co-adsorption are given in Figure 12, and the FTIR bands assignments are reported in Table 6. The results indicate that both Cu^+ and Cu^{2+} cations are present at the surface of materials. But although the Cu^+ cations amount titrated by magnetic measurements remains smaller (33%) than the Cu^{2+}

(34) Hadjiivanov, K. I. *Catal. Rev. Sci. Eng.* **2000**, *42*, 71−144.
(35) Hadjiivanov, K. I.; Vayssilov, G. N. *Adv. Catal.* **2002**, *47*, 308−491.

Table 6. FTIR Band Assignments for Co-adsorption of CO and NO as Probe Molecules

	adsorbed groups identification
NO Adsorption σ (cm^{-1})	
1877	nitrosyl groups $Cu^{2+}-NO$
1315	nitrites (NO^{2-}) on Cu^{2+}, Al^{3+}, and Zn^{2+}
1227	
broad signal: 1454, 1465, 1546, 1630	nitrates NO^{3-} or nitro groups (NO_2) on Cu^{2+}, Zn^{2+}, and Al^{3+}
CO Adsorption σ (cm^{-1})	
2124	carbonyl groups $Cu^{+}-CO$

content (66%), one should have to notice that the quantity of Cu^+ at the surface detected by such a technique remains high. This is consistent with the fact that the Cu^+ cations are preferentially located at the surface, creating oxygen vacancies and defects in these nanoparticles. Moreover the two wavenumbers relating to nitrosyl groups (1877 cm^{-1}) and carbonyl groups (2124 cm^{-1}) are relating to Cu^{2+} and Cu^+, respectively, corresponding to one unique site for each valence state. At the surface, the coordination numbers remain small and correspond probably to tetrahedra.

Impact of the Formation of Defects (Oxygen Vacancies and Monovalent Copper) on the Stoichiometry of Spinels $Zn_{1-x}Cu_xAl_2O_4$. The presence of monovalent copper for the compositions presenting low copper rates has to be compensated in the structure. The occurrence of oxygen vacancies has to be considered in the network while interstitial cations would imply too strong cation−cation interactions.

If oxygen vacancies are present within the network, it has to be mentioned that one oxygen vacancy allows compensating two monovalent copper cations. Moreover, any oxygen atom in the spinel structure is common to three octahedral sites and one tetrahedral site. One oxygen vacancy affects consequently four coordination sites, and locally the three octahedral sites and the tetrahedral site evolve toward three 5-fold coordinated sites and one 3-fold coordinated site.

It is not excluded that these sites undergo a rearrangement toward two 4-fold coordinated sites and two 5-fold coordinated sites. It has to be noticed that the occurrence of divalent copper cations in a 5-fold coordination can besides be partially at the origin of the strong absorption band in the visible range at around 700 nm. Indeed, beautiful green colors are commonly observed for compounds with Cu^{2+} in a square-based pyramid, as it is the case for Y_2BaCuO_5 or Sm_2BaCuO_5[30] with a strong absorption band at around 700 nm (Figure 13). ESR investigations at room temperature on the Y_2BaCuO_5 composition indicate the occurrence of wide anisotropic resonance signal at $g = 2.145$ (Table 7) related to copper cations located in isolated square based pyramids (Figure 14). As 5-fold coordinated copper atoms are well isolated in Y_2BaCuO_5, one can assume that in the case of spinels where some copper cations could occupy 5-fold coordinated sites in interaction with another divalent or monovalent copper, signals relating to Cu^{2+} in 5-fold coordination or in distorded octahedral sites with D_{2h} point groups appear in the same field range with various intensities.

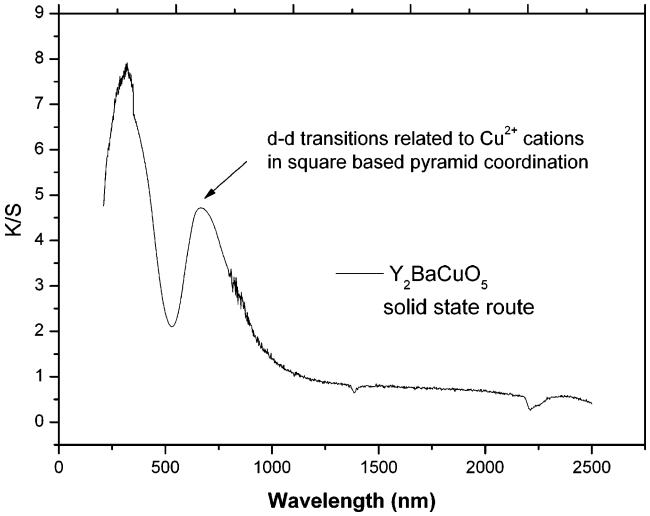

Figure 13. Optical absorption spectrum of Y_2BaCuO_5 obtained by diffuse reflectance.

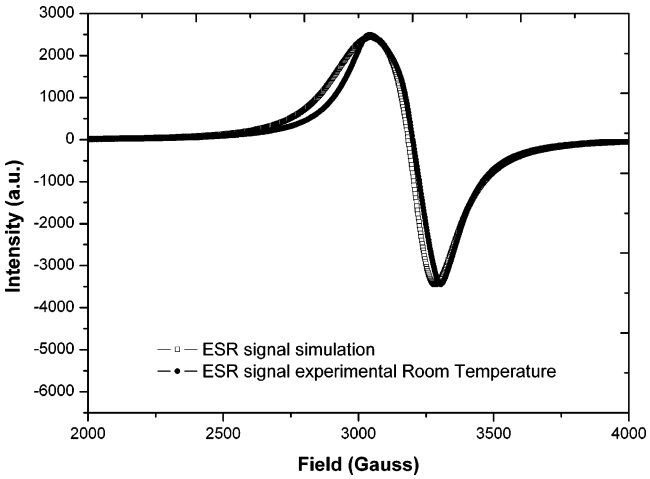

Figure 14. ESR spectrum simulation of Y_2BaCuO_5 obtained by solid-state route.

Table 7. ESR Measurements (g values, hyperfine constants and signal width) of Cu^{2+} in Square-Based Pyramid Environment with C_{4v} Point Group (Case of Y_2BaCuO_5)

pyramid axis	*x*	*y*	*z*
experimental g values	2.09	2.09	2.25
hyperfine constants (Gauss)	0	0	0
signal width (Gauss)	150	150	200

Furthermore, the formation of oxygen vacancies associated with the reduction of the Cu valence state in these nanoparticles considered as metastable phases leads to mention as well the possibility to create cationic vacancies that contribute to increase the number of oxygen vacancies. In the as-prepared "$ZnAl_2O_4$" composition and Al-rich spinel (with Al/Zn atomic ratio larger than 2) compounds, the occurrence of Al^{3+} ions in 5-fold coordination has been demonstrated by ^{27}Al MAS NMR investigations leading to consider oxygen vacancies as well as cationic vacancies to compensate ionic charges. Moreover too low densities that decrease as Al rate increases have been measured using helium pycnometry confirming the occurrence of such defects in these nanoparticles.

It is then clear that this surprising result leading to the oxidation of Cu^{+} at high temperature is due to the creation of defects at low temperature in these nanoparticles allowing the stabilization of high content of monovalent copper (33%) in tetrahedral sites forming pairs with Cu^{2+} in *Td* (4-fold coordination), C_{4v} (5-fold coordination), and D_{2h} (6-fold coordination) symmetry. Then the formation of electronic $Cu^{+}-Cu^{2+}$ pairs allow stabilizing a high content of defects such as oxygen as well as cationic vacancies with a maximum rate reached at $x = 1/6$ corresponding to the situation where the probability to get isolated $Cu^{+}-Cu^{2+}$ pairs in Td and Oh sites respectively becomes the highest.

From $x > 1/6$, in the case of the $x = 0.20$ composition for instance, the Cu^{+} content is very low because the $Cu^{2+}-Cu^{2+}$ interactions become more and more important leading to the destabilization of monovalent copper in tetrahedral site. From $x \geq 0.30$, the formation of Cu^{0} and CuO is due to the high rate of defects such as oxygen vacancies mainly generated at the surface of these nanoparticles and the capability of copper to be reduced. The zinc aluminate framework cannot accommodate a too large content of Cu^{+}, and the limitation of constrains within the network is at the origin of the disproportionation reaction of monovalent copper.

Suitable techniques such as XRD, TEM, ESR, magnetic measurements, and finally UV−vis−NIR spectroscopy allow showing on one hand the clear differences between samples obtained by solid-state route[23] and this low-temperature preparative method. Moreover, if these characterizations correspond to a bulk analysis, the co-adsorption of probe molecules at the surface and the FTIR spectra show the occurrence of mixed Cu^{+I}/Cu^{+II} valence states stabilized at the surface. X-ray photoelectron spectroscopy (XPS) measurements could also give access to such results. Thanks to the stabilization of nanosized particles, it is reasonable to assume that low valence states of copper associated to oxygen defects or vacancies are mainly stabilized at the surface due to the reduction of Madelung potentials. On the other hand, one should have to point out this synthesis route allows preparing in a reproducible way nanocrystallized phases. The occurrence of mixed valency coupled with oxygen defects stabilized into nanoparticles exhibiting high surface area as well as the stabilization of metal copper due to a disproportionation reaction at the surface are probably key factors for developing performing and valuable redox catalysts during cycles between oxidative and reductive atmospheres.[36]

Conclusions

The synthesis of $Zn_{1-x}Cu_xAl_2O_4$ spinel series by low-temperature process is possible and leads to the obtention of highly divided crystalline powders, whose color evolves with the copper content. For $x \geq 0.30$, traces of CuO and metallic copper are stabilized and their presence is explained by the disproportionation reaction of monovalent copper according to the Ellingham diagram. The evolution of the structural features in this series is almost similar to what is observed for the solid solution obtained by conventional solid-state route. Nevertheless, similar inversion rates and slightly lower cell parameters are observed for samples obtained by this low-temperature process compared to those obtained by solid-state route. Furthermore, for $x = 0.15$ composition, the a cell parameter reaches clearly its maximum.

The stabilization of nanoparticles with a large content of defects associated to the reduction of Madelung potentials on each sites and the reductive properties of the polyesterification route involving citric acid and ethylene glycol are doubtless at the origin of the occurrence of a mixed valency for copper in the case of compositions containing the low amount of copper ($x < 1/6$). Especially for the composition $x = 0.15$, a high content of Cu^{+} cations (33%) is identified as well as a strong variation of the absorption band centered at around 700 nm compared to the same composition obtained by solid-state route. Magnetic measurements and ESR spectra evolution for compounds prepared by the two routes, function of the annealing temperature for the low-temperature preparative method, and finally the identification of Cu valence state by FTIR analysis of the co-adsorption of probe molecules, lead to conclude certainly to the evidence of monovalent copper in the spinel network.

Two hypotheses are finally proposed to explain the dependence of this absorption band intensity versus the synthesis route. Either this dependence is directly linked to the presence of monovalent copper cations stabilized through the polyesterification reaction, since intervalency transitions or intra-atomic transitions occur in this wavelength range. Or this is indirectly linked to the presence of monovalent copper. Indeed, the occurrence of a mixed valency for copper cations implies the presence of oxygen vacancies in the anionic network. Locally divalent copper cations could be stabilized in a 5-fold coordination, giving rise to intra-atomic d−d transitions with high probability at around 700 nm. Finally, it is important to conclude that the surprising fact showing an oxidation reaction of monovalent copper at high temperatures is due to the stabilization of defects within the spinel framework at low temperature, such as oxygen vacancies allowing and leading to the formation of Cu^{+} in Td symmetry. This metastable phase containing oxygen vacancies and monovalent copper evolves to thermodynamically stabilized phase with only divalent copper and a limitation of oxygen vacancies. Based on these conclusions, a new zinc aluminate spinels series presenting high excess of aluminum cations as well as high degree of anionic and cationic vacancies has been prepared and is under investigations on a structural point of view.

Acknowledgment. The authors thank Dr. Michel Ménétrier and Dr. Alexandrine Flambard for the ^{27}Al NMR experiments. They also thank Agfa-Gevaert, IWT, and CNRS for financial support.

IC0624064

(36) Nishita, Y.; Mizuki, J.; Akao, T.; Tanaka, H.; Uenishi, M.; Kimura, M.; Okamoto, T.; Hamada, N. *Nature* **2002**, *418*, 164.
(37) Abragam, A.; Bleaney, B. *Electron Paramagnetic Resonance of Transition Ions*; Dover Publications: New York, 1986.